X-Ray Diffraction Study of Amorphous $CeFe_2H_3$ and $GdFe_2H_3$ Alloys Produced by Hydrogenation

E. Matsubara, Y. Ohzora, and Y. Waseda
The Research Institute of Mineral Dressing and Metallurgy (SENKEN), Tohoku University, Sendai 980, Japan

K. Aoki, K. Fukamichi, and T. Masumoto
The Research Institute for Iron, Steel, and Other Metals, Tohoku University, Sendai 980, Japan

Z. Naturforsch. **42 a**, 582–586 (1987); received November 18, 1986

The structure of amorphous $CeFe_2H_3$ and $GdFe_2H_3$ alloys produced by hydrogenation is investigated and compared with that of amorphous $CeFe_2$ and $GdFe_2$ produced by high-rate DC sputtering. Distinct different structural features, characterized by an almost resolved first peak of the RDF of the former were found.

Introduction

Amorphous alloys can be produced by rapid quenching from the melt or by vapor deposition at rates sufficient to bypass crystallization. On the other hand, Yeh, Samwer and Johnson [1] reported in 1983, the formation of amorphous alloys by solid state reactions. In these methods, the amorphous alloys can be formed more slowly than by the conventional techniques. In [1] it was found that amorphous hydrides can be formed by the reaction of crystalline intermetallic compounds with gaseous hydrogen. Subsequently it has been demonstrated [2, 3] that inter-diffusion among thin multi-layers of binary alloys can produce a single phase amorphous film.

Unlike rapid quenching from melts or vapor deposition, there is no restriction as to the dimensions of the amorphous samples produced by solid state reactions. Several amorphous alloys have already been produced by these new techniques [4, 5]. However, to the best of our knowledge the structure of such amorphous alloys has not yet been extensively studied.

In this paper we describe our systematic x-ray diffraction study on amorphous $CeFe_2H_3$ and $GdFe_2H_3$ alloys produced by hydrogenation.

Reprint requests to Dr. E. Matsubara, Research Institute of Mineral Dressing and Metallurgy (SENKEN), Tohoku University, Sendai 980, Japan.

Experimental

The amorphous $CeFe_2H_3$ and $GdFe_2H_3$ alloys were synthesized by exposing pulverized crystalline $CeFe_2$ and $GdFe_2$ (Laves phases), respectively, to high purity hydrogen gas (7N) of 5 MPa in a stainless steel reactor 300 K and 573 K, respectively. The samples obtained measured 30 to 80 μm in diameter. The amorphous $CeFe_2$ and $GdFe_2$ alloys were prepared by high-rate DC sputtering in the form of plates about 0.4 mm thick. For the x-ray measurements, their faces were mechanically polished with a $MgO-H_2O$ slurry. Details of the sample preparation are described in [5] and [6].

The x-ray scattering intensities from the samples were measured using a diffractometer whose x-ray tube and detector rotate at the same angular velocity in opposite directions about the horizontal axis. For details of this technique cf. [7, 8].

A molybdenum x-ray tube and a singly-bent pyrolytic graphite monochromator in the diffracted beam were used. The intensity profile was obtained from 3° to 60°, which corresponds to a wavevector $Q = 4\pi \sin\theta/\lambda$ from 9 to 153 nm^{-1}, where λ is the wavelength and 2θ is the angle between the incident and diffracted x-rays. In order to obtain the same statistical error for every measured point, a fixed-count mode was applied and at least 20,000 counts were collected. It took at least a couple of days to measure a whole intensity profile. The samples except $CeFe_2H_3$ were measured in air while $CeFe_2H_3$ was maintained in argon gas with 7%

0932-0784 / 87 / 0600-0582 $ 01.30/0. – Please order a reprint rather than making your own copy.

hydrogen in order to prevent its oxidation, which mainly results from the high chemical reactivity of Ce. Some oxidation could still occur during a measurement for a couple of days. Therefore the measurements on $CeFe_2H_3$ were performed during about 12 hours only and repeated four times. In each measurement, at least 7000 counts were collected. The average was about 10,000 counts. Consequently, the statistical counting error was $\pm 4.8\%$ at most, which is worse than the error $\pm 0.5\%$ obtained for the other amorphous alloys, where the measurements lasted about four times longer. In this way, if any oxidation did occur, it would have been detected by comparing the four intensity profiles obtained. Systematic changes of the intensities could not be found, the variations of the intensities having been at most $\pm 0.9\%$. This is within the statistical counting error. Therefore the sum of the intensities of the four measurements was used in the data analysis of $CeFe_2H_3$.

The polarization correction for an ideal monochromator has been applied, and the Compton scattering was corrected using the values reported by Cromer and Mann [9] and the so-called Breit-Dirac recoil factors. In order to convert the observed intensities into electron units, the generalized Krogh-Moe-Norman method [10] was used with atomic scattering factors tabulated in [11] including the anomalous dispersion corrections [12]. In this work, the observed intensity data at Q values $< 10\,\mathrm{nm}^{-1}$ have been smoothly extrapolated to $Q = 0$. The effect of the extrapolation and the truncation up to $Q = 153\,\mathrm{nm}^{-1}$ is known to give no critical contribution in the calculation of the radial distribution function (RDF) by the Fourier transformation [7, 8]. The RDF is evaluated from the total structure factor $S(Q)$ for a non-crystalline system containing more than two kinds of atoms by the equation

$$4\pi r^2 \varrho(r) = 4\pi r^2 \varrho_0 + \frac{2r}{\pi} \int_0^\infty Q\,[S(Q) - 1] \sin(Q r)\, \mathrm{d}Q\,, \quad (1)$$

$$S(Q) = [I_{\mathrm{eu}}^{\mathrm{coh}}(Q) - \langle f^2 \rangle + \langle f \rangle^2] / \langle f \rangle^2\,, \quad (2)$$

where $I_{\mathrm{eu}}^{\mathrm{coh}}(Q)$ is the coherent x-ray scattering intensity in electron units per atom, which is directly determined from the scattering experiments. $\langle f \rangle$ is the average atomic scattering factor and $\langle f^2 \rangle$ is the average of its square. $\varrho(r)$ is the averaged radial density function and ϱ_0 is the average number density of atoms.

Results and Discussion

Figure 1 shows the x-ray scattering intensity pattern of amorphous $CeFe_2H_3$. The profile corresponds to a typical non-crystalline structure and consists of a relatively sharp first peak followed by small diffuse peaks. As seen in Fig. 1, many "spikes" appear on the broad peaks. In order to identify these, x-ray scattering measurements on pulverized crystalline $CeFe_2$ were carried out (cf. Figure 1). The resulting diffraction pattern is a mixture of Bragg peaks from $CeFe_2$ (Laves phase) and CeO_2. By comparing the two profiles in Fig. 1, it is found that most of the small "spikes" on the $CeFe_2H_3$ profile are due to CeO_2. This may imply that, because of the high chemical reactivity of Ce, the formation of CeO_2 is unavoidable in the production process of the mother alloy $CeFe_2$ from pure Ce and Fe, and this oxide is unchanged by the hydrogenation, so that the peaks corresponding to CeO_2 are still

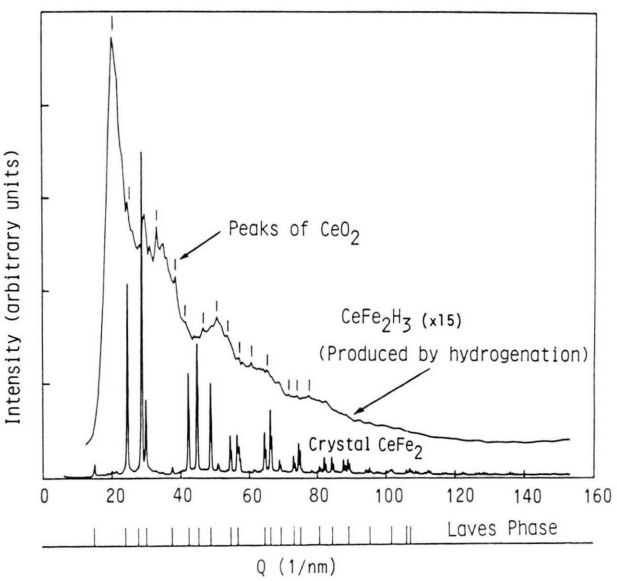

Fig. 1. X-ray diffraction patterns for amorphous $CeFe_2H_3$ and the crystalline Laves phase $CeFe_2$. Lines on the amorphous profile indicate positions of Ce oxide peaks. Peak positions of the crystalline Laves phase are indicated below the abscissa.

present in the diffraction pattern of the amorphous $CeFe_2H_3$. Evidently the original Bragg peaks from the crystalline $CeFe_2$ (Laves phase) are substantially reduced by the hydrogenation but can still be noticed in some cases. This suggests that the hydrogenation, depending upon time and temperature, was not complete. Therefore, the x-ray scattering intensity data of the pulverized crystalline $CeFe_2$ mother alloy were used in the background subtraction process for the amorphous $CeFe_2H_3$ alloy, so that the sharp Bragg peaks corresponding to the $CeFe_2$ phase were excluded.

In this way the x-ray scattering intensity from pure amorphous $CeFe_2H_3$ was obtained. Similarly, a small amount of Gd_2O_3 and the crystalline Laves phase of $GdFe_2$ existed in the amorphous $GdFe_2H_3$ alloy, and the corresponding intensities were substracted to obtain the profile of the pure amorphous $GdFe_2H_3$. The resultant structure factors $S(Q)$ of $CeFe_2H_3$ and $GdFe_2H_3$ as well as of $CeFe_2$ and $GdFe_2$ are given in Figs. 2 and 3, respectively. The present results for amorphous sputtered $CeFe_2$ and $GdFe_2$ are in good agreement with the work reported by Matsuura et al. [13]. The $CeFe_2$- and $GdFe_2$-structure factors in Fig. 3 show only a first and second peak, however no third, fourth and so on peak and also no splitting up of the second peak. Thus these patterns are rather unlike those which normally are obtained with amorphous binaries.

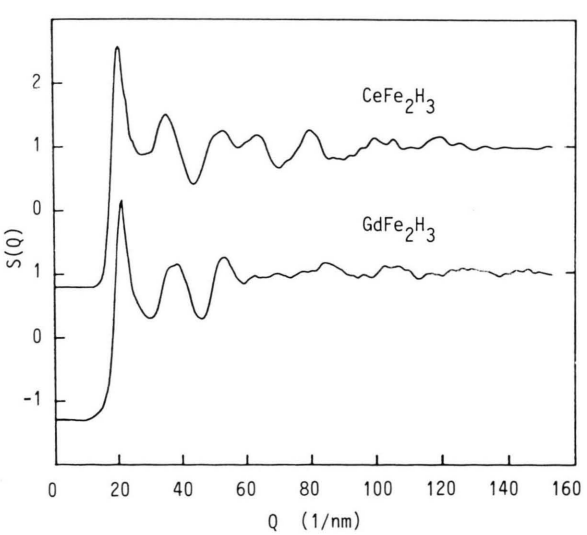

Fig. 2. Total structure factors $S(Q)$ of amorphous $CeFe_2H_3$ and $GdFe_2H_3$.

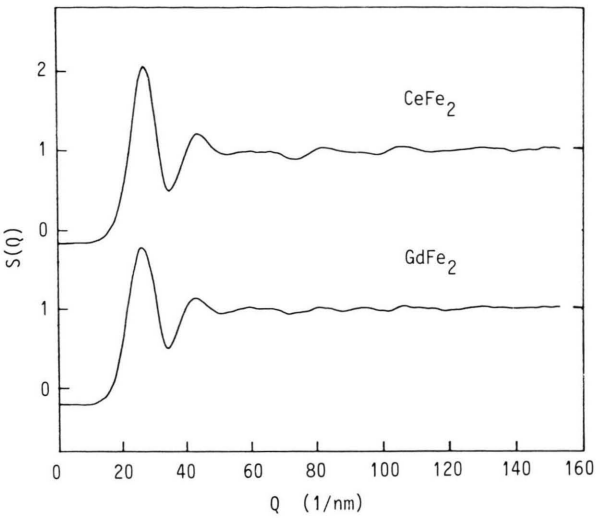

Fig. 3. Total structure factors $S(Q)$ of amorphous sputtered $CeFe_2$ and $GdFe_2$ alloys.

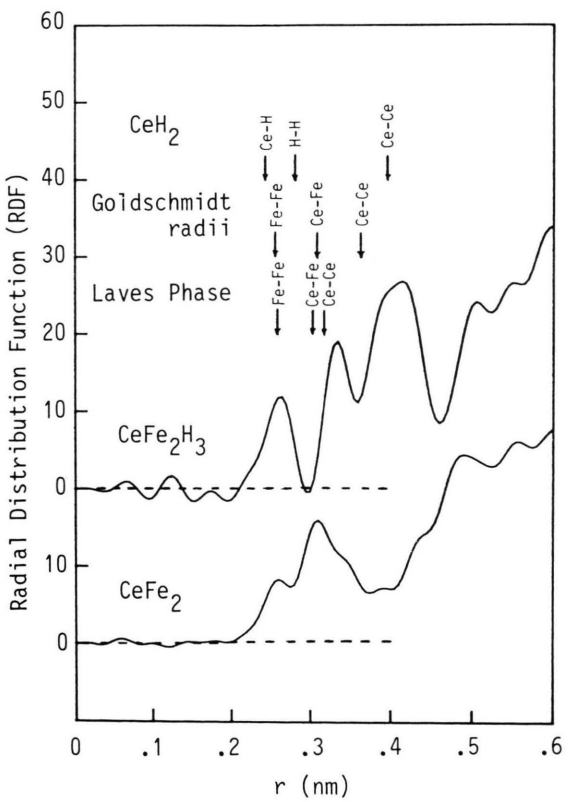

Fig. 4. Radial distribution functions of amorphous $CeFe_2H_3$ (Density = 5.40 g/cm^3) and $CeFe_2$ (Density = 8.98 g/cm^3). Arrows indicate positions of Fe–Fe, Fe–Ce, and Ce–Ce distances calculated from a crystalline hydride phase CeH_2, from Goldschmidt radii, and from a crystalline Laves phase $CeFe_2$, respectively.

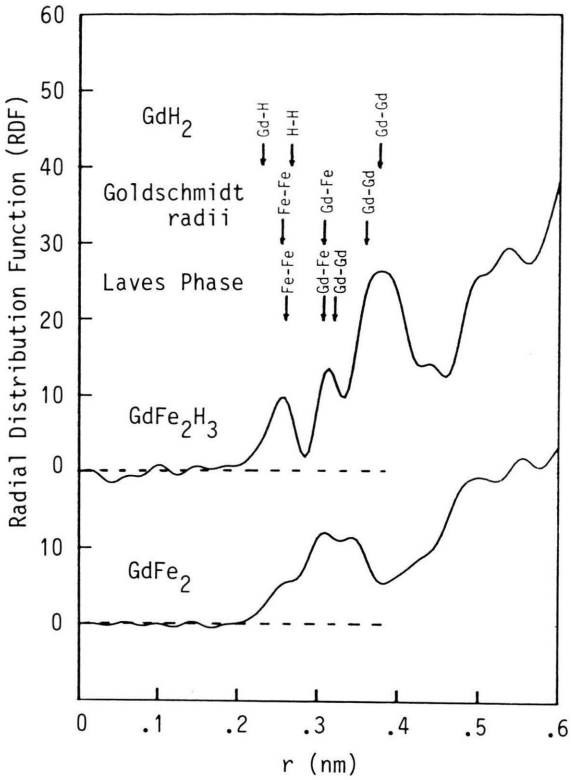

Fig. 5. Radial distribution function of amorphous $GdFe_2H_3$ (Density = 6.19 g/cm^3) and $GdFe_2$ (Density = 7.84 g/cm^3). Arrows indicate positions of Fe–Fe, Fe–Gd, and Gd–Gd distances calculated from a crystalline hydride phase GdH_2, from Goldschmidt radii, and from a crystalline Laves phase $GdFe_2$, respectively.

The same conclusion stands for the structure factors of amorphous $CeFe_2H_3$ and $GdFe_2H_3$ as shown in Fig. 2 where the oscillations are still distinct in the high Q region while the structure factors of $CeFe_2$ and $GdFe_2$ are damped more rapidly. This qualitatively indicates that a certain short range order, different from that obtained in typical amorphous alloys, is present in the amorphous $CeFe_2H_3$ and $GdFe_2H_3$ alloys, indicating the presence of species with definite bond lengths and angular relations [14].

The radial distribution functions (RDFs) calculated by (1) are shown in Figs. 4 and 5. The nearest neighbour distances, as evaluated from the Goldschmidt radii [15], from the crystalline Laves phases $CeFe_2$ and $GdFe_2$ [16], and from the crystalline hydride phases CeH_2 and GdH_2 [16] are indicated in Figs. 4 and 5. The spurious ripples in the small r region are meaningless: the RDF is essentially zero inside the atomic diameter. The peak positions were determined from the position of the apex parabolas through three points near the corresponding peak maximum. The first three neighbour distances in amorphous $CeFe_2$ are considered to be due to the Fe–Fe-, Fe–Ce-, and Ce–Ce-pairs. The same stands for amorphous $GdFe_2$; one only has to replace Ce by Gd. For the evaluation of the coordination numbers the shape of the peaks was assumed to be Gaussian. The results are summarized in Table 1, together with the values calculated from the crystalline Laves phases [16].

Table 1. Comparison of coordination numbers, N, and interatomic distances, r, for amorphous sputtered $CeFe_2$ and $GdFe_2$ obtained in this study with those calculated from crystalline Laves phase data [16]. N_{Fe-Fe}, N_{Fe-Ce}, and N_{Ce-Ce} are experimental values. N_{Ce-Fe} was calculated according to $N_{Ce-Fe} = \left(\frac{C_{Fe}}{C_{Ce}}\right) N_{Fe-Ce}$. C_{Fe} and C_{Ce} being the atomic fractions. The corresponding calculation was done for N_{Gd-Fe}.

$CeFe_2$				
Atomic Pair	Amorphous Phase		Laves phase	
	N	r (nm)	N	r (nm)
Fe–Fe	9.6	0.258	6	0.258
Fe–Ce	4.9	0.309	6	0.303
Ce–Fe	9.9	0.309	12	0.303
Ce–Ce	4.2	0.350	4	0.316
$GdFe_2$				
Atomic Pair	Amorphous Phase		Laves phase	
	N	r (nm)	N	r (nm)
Fe–Fe	7.4	0.258	6	0.261
Fe–Gd	3.6	0.307	6	0.307
Gd–Fe	7.3	0.307	12	0.307
Gd–Gd	4.8	0.349	4	0.320

Taking into account that the determination of the first coordination number is uncertain with an error of ± 10% we only learn that the atomic arrangement in the Laves phase and the corresponding amorphous phase is different. In ternary systems there are six kinds of pairs. Since in the present case one of the components, namely H can be neglected because of its very poor scattering power for X-rays, only the Fe–Fe-, Fe–Ce-, and Ce–Ce-pairs in the case of $CeFe_2H_3$ as well as only the Fe–Fe-, Fe–Gd-, and Gd–Gd-pairs in the case of $GdFe_2H_3$ can contribute to the RDF. In both cases the first peak is caused by Fe–Fe-pairs, as suggested in

Figs. 4 and 5, and the coordination number is estimated to be about seven in both cases. The following structural features can be derived from the present results for amorphous $CeFe_2H_3$ and $GdFe_2H_3$.

As seen in the RDF curves of Figs. 4 and 5, the peak at 0.4 nm is higher than the first and second ones in RDFs for amorphous $CeFe_2H_3$ and $GdFe_2H_3$. The oscillations rapidly decay and the RDF shows no structurally significant deviations from the average value of $4\pi r^2 \varrho_0$ at $r > \approx 0.65$ nm in both systems. This type of atomic configuration in non-crystalline systems corresponds to distinct local nearest neighbour correlations, as seen in semiconducting liquids (Te and Se) and oxide glasses [8], accompanied by a complete loss of correlation between such units at larger distances. The Ce–Ce- and Gd–Gd-distance at 0.4 nm, which also occurs in CeH_2 and GdH_2, forms the dominant feature in $CeFe_2H_3$ and in $GdFe_2H_3$ and indicates a certain relationship between CeH_2 and GdH_2 on the one as well as $CeFe_2H_3$ and $GdFe_2H_3$ on the other side. In both cases Fe–Fe-pairs are indicated as first maximum. The second maximum fits well to Gd–Fe and Gd–Gd which is shifted to larger r-values in the case of $GdFe_2H_3$. However, it should be kept in mind that the origin of the characteristic structural features in amorphous $CeFe_2H_3$ and $GdFe_2H_3$ cannot be identified with certainty since at the present time partial correlation functions are not available.

Acknowledgements

The authors (EM and YW) would like to thank the Research Laboratories, UNITIKA Ltd. and the Kawasaki Steel Corporation, Technical Research Division for their financial support.

[1] X. L. Yeh, K. Samwer, and W. L. Johnson, Appl. Phys. Lett. **42,** 242 (1983).
[2] R. Schwartz and W. L. Johnson, Phys. Rev. Lett. **51,** 415 (1983).
[3] M. Van Rossum, M. A. Nicolet, and W. L. Johnson, Phys. Rev. **B29,** 5498 (1984).
[4] For example, W. L. Johnson, Proc. 5th Inter. Conf. on Rapidly Quenched Metals, Wurzburg (1984), North-Holland, Amsterdom 1985, p. 1515.
[5] K. Aoki, K. Shirakawa, and T. Masumoto, Sci. Rep. Res. Inst. Tohoku University **32 A,** 231 (1985).
[6] T. Satoh, K. Fukamachi, and Y. Satoh, Sci. Rep. Res. Inst. Tohoku University **32 A,** 190 (1985).
[7] C. N. J. Wagner, J. Non-Cryst. Solids **31,** 1 (1978).
[8] Y. Waseda, The structure of Non-Crystalline Materials, McGraw-Hill, New York 1980.
[9] D. T. Cromer and J. B. Mann, J. Chem. Phys. **47,** 1892 (1967).
[10] C. N. J. Wagner, H. Ocken, and M. L. Joshi, Zeit. Naturforsch. **20 a,** 325 (1965).
[11] International Tables for X-ray Crystallography, Vol. IV, The Kynoch Press, Birmingham 1974.
[12] D. T. Cromer and D. Libermann, J. Chem. Phys. **53,** 1891 (1970).
[13] M. Matsuura, T. Fukunaga, K. Fukamichi, and K. Suzuki, Proc. 6th Inter. Conf. on Liquid and Amorphous Metals, Garmisch (1986), Paper No. Mo 11, in press.
[14] P. A. Egelstaff, D. I. Page, and J. G. Powles, Mol. Phys. **20,** 881 (1971).
[15] V. M. Goldschmidt, Geochemistry, Oxford, London 1954.
[16] W. B. Pearson, Handbook of Lattice Spacing and Structure of Metals, Pergamon Press, New York 1967.